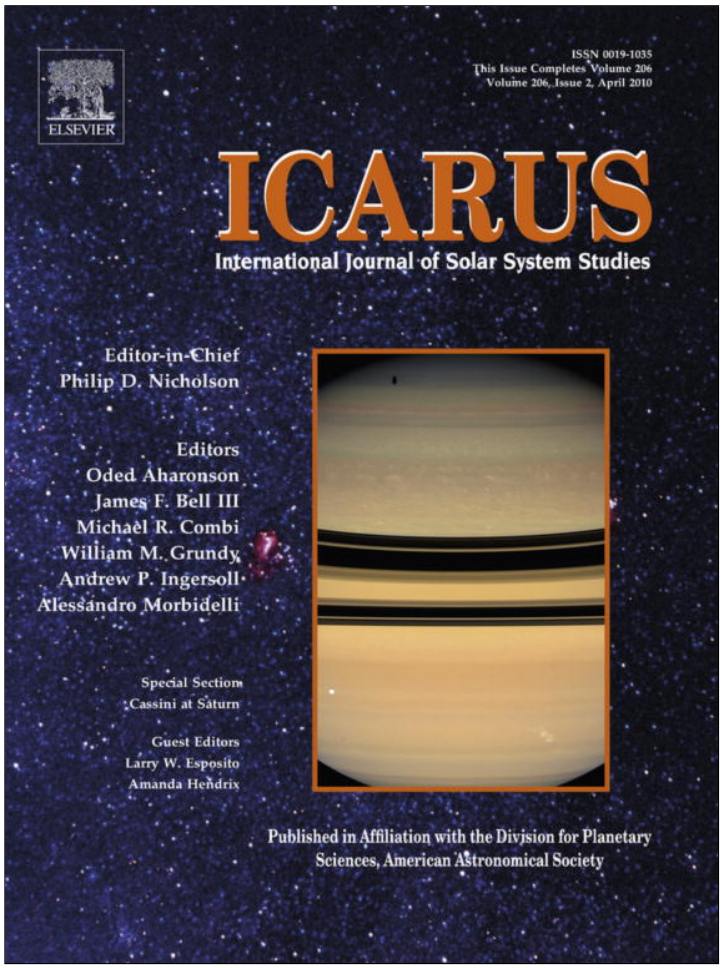

Icarus 206 (2010) 410–423

Contents lists available at ScienceDirect

Icarus

journal homepage: www.elsevier.com/locate/icarus

Self-gravity wake parameters in Saturn's A and B rings

P.D. Nicholson *, M.M. Hedman

Department of Astronomy, Cornell University, Ithaca, NY 14853-6801, USA

ARTICLE INFO

Article history:
Received 25 December 2008
Revised 22 July 2009
Accepted 23 July 2009
Available online 28 July 2009

Keywords:
Planetary rings
Saturn, rings
Occultations

ABSTRACT

An increasing body of evidence shows that, at the sub-km level, Saturn's main A and B rings are dominated by an ever-changing pattern of elongated, canted structures known as self-gravity wakes. Best known for causing azimuthal variations in the rings' reflectivity, these structures also have a profound influence on how the transmission of the rings varies with both longitude and opening angle, B (Colwell et al. [2006] Geophys. Res. Lett. 33, 7201; Colwell et al. [2007] Icarus 190, 127–144; Hedman et al. [2007] Astron. J. 133, 2624–2629). We use data from three stellar occultations observed by *Cassini*'s Visual and Infrared Mapping Spectrometer (VIMS) to measure the transmission of the rings as a function of B, when viewed parallel to the wakes. These data are used to constrain properties of the self-gravity wakes as a function of radius across the A and B rings: specifically the fractional width of the gaps between the wakes, G/λ, and the average normal optical depth in the gaps, τ_G. We find that the overall normal optical depth of the rings, τ_n is primarily controlled by G/λ, which varies between <0.05 and ~0.70 in the A and B rings. The gaps, however, are not completely empty, being filled by material — possibly cm-sized ring particles — with an average normal optical depth which varies from 0.12 to ~0.4. In addition to regional variations, local variations in τ_G are seen in the regular structure which dominates the inner B ring, and in the environs of strong density waves in the A ring. The same model applied to the lower optical depth Cassini Division reveals very little evidence of self-gravity wakes, except where τ_n exceeds ~0.25.

1. Introduction

Saturn's A ring shows clear azimuthal variations in its visible and microwave reflectivity and infrared emissivity (Lumme and Irvine, 1976, 1984; Reitsema et al., 1976; Lumme et al., 1977; Thompson et al., 1981; Franklin et al., 1987; Dones et al., 1993; Dunn et al., 2004; Nicholson et al., 2005; French et al., 2007; Porco et al., 2008; Ferrari et al., 2009). Although much weaker than those in the A ring, similar quadrupole asymmetries have also been reported in the B ring at both optical (French et al., 2007) and radar (Nicholson et al., 2005) wavelengths. In all cases, minima in reflectivity and emissivity are observed at longitudes of ~70° and ~250° with respect to the observer. These quadrupole variations are generally attributed to what are now commonly referred to as 'self-gravity wakes' (Colombo et al., 1976; Franklin and Colombo, 1978; Dones and Porco, 1989). These sub-kilometer-scale structures arise spontaneously as a result of gravitational perturbations in a shearing disk, and are the smaller cousins of similar features originally studied in the context of galactic disks by Julian and Toomre (1966). (See Toomre and Kalnajs (1991) for a more recent discussion and numerical examples.) Brightness minima in the rings occur where the trailing wakes are seen end-on and thus present their minimum cross-section to the observer.

Numerical simulations of Saturn's rings which incorporate both self-gravity and inelastic collisions predict the spontaneous development of self-gravity wakes with a characteristic separation close to the critical wavelength for radial instability in a self-gravitating disk (Toomre, 1964):

$$\lambda_{crit} = 4\pi^2 G\sigma/\Omega^2 \quad (1)$$

where σ is the surface mass density of the ring and Ω is the local orbital angular velocity. Wakes develop as long as the disk's Toomre instability parameter, $Q \leqslant 2$ (Salo, 1992a,b, 1995; Daisaka and Ida, 1999). In Saturn's A ring, $\lambda_{crit} \simeq 60$ m, or about 10 times the radius of the largest ring particles.

Recent numerical simulations combined with Monte Carlo light-scattering models by Salo et al. (2004) and French et al. (2007) show quantitatively that the self-gravity wakes in Saturn's rings are indeed able to match the amplitude and phase of the azimuthal asymmetry seen in Voyager and HST images of the A ring, using plausible phase functions and particle size distributions based on Voyager radio occultation data (Zebker et al., 1985).

With the advent of multiple stellar and radio occultations by the rings observed by the *Cassini* spacecraft, it is now possible to probe the properties of self-gravity wakes in much greater detail by their effects on the transmission of the rings. Simple numerical and ana-

* Corresponding author.
E-mail addresses: nicholso@astro.cornell.edu, icarus@astro.cornell.edu (P.D. Nicholson).

0019-1035/$ - see front matter © 2009 Elsevier Inc. All rights reserved.
doi:10.1016/j.icarus.2009.07.028

lytic models fitted to stellar occultation data returned by the Ultraviolet Imaging Spectrometer (UVIS) and Visual and Infrared Mapping Spectrometer (VIMS) instruments have led to generally-consistent estimates of the average orientation, width and vertical thickness of the wakes, as well as some indication of the variations in these parameters across the A ring (Colwell et al., 2006, 2007; Hedman et al., 2007). Radio occultations at different longitudes also show strong evidence for wakes in the A ring (Marouf et al., 2006b) and in parts of the B ring (Marouf et al., 2007), though quantitative results are not yet available.

Besides leading to azimuthal variations in ring reflectivity, thermal emissivity and transmission, self-gravity wakes are also expected to have a marked effect on the variation of these same quantities with ring opening angle. Traditional optical and infrared photometric models have treated the rings as a homogeneous, many-particle-thick layer of independently scattering or emitting particles which is characterized by its normal optical depth:

$$\tau(\lambda) = \int_{r_{\min}}^{r_{\max}} \pi r^2 Q(r,\lambda)\; n(r)\; dr \tag{2}$$

where $n(r)$ is the differential particle size distribution per unit area of the rings, assumed to extend from $r_{\min}$ to $r_{\max}$, and $Q(r,\lambda)$ is the particle's extinction efficiency at wavelength λ. The transmission of such a ring at an opening angle B is determined by the slant optical path length through the rings:

$$T(B) = e^{-\tau/\sin|B|}. \tag{3}$$

The real rings, however, do not obey such a simple model. Colwell et al. (2007) have used UVIS stellar occultation data to show that, especially in the B ring, the actual transmission does not decrease nearly as rapidly for low values of B as Eq. (3) would imply. The same effect is seen in the A ring, but to a lesser degree.[1]

This behaviour is a natural consequence of the presence of self-gravity wakes, which result in an essentially bimodal distribution of optical depths on a sub-km scale. Consider an idealized ring composed of infinitely flat and essentially opaque self-gravity wakes, of average width W, separated by empty gaps of average width G. Such a ring will have a transmission — when averaged over a spatial scale much greater than the wavelength of the wakes — equal to $G/(W+G)$. This transmission is *independent* of B, and would lead to an *apparent* normal optical depth, computed using Eq. (3), of

$$\tau_{\rm n} = -\sin|B|\ln(T), \tag{4}$$

which is proportional to $\sin B$. Indeed, Colwell et al. (2007) found that $\tau_{\rm n}$ does increase monotonically with ring opening angle in the A and B rings, though not linearly as this simple model implies. However, they were able to account for the observed variation of $\tau_{\rm n}$ with B and longitude using a simple model of three-dimensional, opaque wakes separated by partially-transparent gaps.

In this paper we report on a similar analysis of VIMS stellar occultation data for Saturn's rings, with the goal of refining the properties of the self-gravity wakes in both the A and B rings. In particular, we seek to constrain the widths and optical depths of the gaps between the wakes, and their variation with radius. In our earlier study of self-gravity wakes in the VIMS data (Hedman et al., 2007), we used multiple occultations of the star *o* Ceti to map out the variation in transmission with longitude across the A ring, keeping B constant, from which we were able to determine the orientation of the wakes and their vertical thickness, H, as a fraction of their average wavelength, independent of other assumptions. In the present work, we take an orthogonal approach and use multiple stars to examine the variation in transmission with B, at a constant azimuthal orientation relative to the observer. By carefully choosing a few occultations whose tracks crossed the rings at longitudes near the maximum in wake transmission, our measurements are sensitive to the width and optical depth of the interwake gaps, but insensitive to the three-dimensional shape and optical thickness of the wakes themselves. Our results are consistent with those reported by Colwell et al. (2007), but by examining only a selected subset of the available data and confining our attention to only two model parameters we find much less scatter in these parameters and are thus able to see more subtle correlations with other characteristics of the rings.

The paper is organized as follows. In Section 2 we describe our analytical model for self-gravity wakes, while the observations and data reduction are summarized in Sections 3 and 4. Our results are presented in detail in Section 5, and summarized in Section 6. Details of the data reduction for each occultation used here are presented in Appendix A, for future reference.

2. The model

Our motivation for looking at a restricted subset of the occultations stems from a simplified model of the wakes as infinitely-long, straight, parallel, regularly-spaced, opaque elliptical cylinders with height H and width W, as described by Hedman et al. (2007). These cylinders are separated by gaps of width G and line-of-sight transmission $T_G = e^{-\tau_G/\sin|B|}$. For an occultation with a ring opening angle of B and a viewing direction relative to the wakes of $\theta = \phi - \phi_W$, the average transmission is given by:

$$T(\theta) = T_G\left[1 - \sqrt{\left(\frac{H\sin\theta}{\lambda\tan B}\right)^2 + \left(\frac{W}{\lambda}\right)^2}\right], \tag{5}$$

where here $\lambda = G + W$ is the overall wavelength of the wake structure.[2] The angle ϕ is measured in a prograde direction from the line of sight to the star, projected onto the ring plane, to the local radial direction; it is also equal to the longitude of the point on the occultation track relative to the stellar direction. The orientation or pitch angle of the wakes, measured from the local radial direction, is denoted by $\phi_{\rm W}$, with positive values denoting trailing wakes.

Numerical simulations of self-gravity wakes in the A ring predict a mean pitch angle of $\phi_{\rm W} \simeq 69^\circ$ (Salo et al., 2004). Observationally, Hedman et al. (2007) found that $64^\circ < \phi_W < 73^\circ$ across the A ring, while Colwell et al. (2007) obtained a wider range of $45^\circ < \phi_W < 80^\circ$ in the A ring and $60^\circ < \phi_W < 90^\circ$ in the B ring. From thermal emissivity variations, Ferrari et al. (2009) determined that the average value of $\phi_{\rm W}$ in the A ring is $70.7 \pm 0.7^\circ$. For modelling purposes, we will assume that $\phi_W = 70^\circ$ in both A and B rings.

If we now restrict our attention to observations for which the stellar line of sight is roughly parallel to the wakes, then $\sin\theta \simeq 0$ and this expression reduces to:

$$T(\theta = 0) = T_G\frac{G}{\lambda} = \frac{G}{\lambda}e^{-\tau_G/\sin|B|}, \tag{6}$$

[1] The C ring, by contrast, appears to show no azimuthal asymmetries and to follow Eq. (3) quite closely.

[2] This model is, of course, highly-idealized in comparison with the real rings. A recent study of N-body simulations of self-gravity wakes by Tiscareno et al. (2009) shows that the distribution of local optical depths is better described as trimodal, rather than bimodal, with up to 50% of the ring's surface area exhibiting a normal optical depth as low as 0.01. The remaining area is occupied by essentially-opaque wakes and a transitional zone of intermediate optical depth. However, these authors find that stellar occultation experiments can only distinguish between bimodal and trimodal distributions at very low opening angles, and that τ_G can be interpreted as an area-weighted average optical depth of the regions between the wakes.

which is valid as long as $\sin\theta \ll \frac{W}{H}\tan B$. Defining the apparent normal optical depth, τ_n, as in Eq. (4) above, this equation can be rewritten as:

$$\tau_n = \tau_G - \ln(G/\lambda)\sin|B|. \quad (7)$$

If we have two measurements of τ_n at two different opening angles, we can determine both the optical depth in the gaps, τ_G, and the gap fraction, G/λ. Fig. 1 illustrates the predicted variations of T and τ_n with $\sin B$ for several representative values of τ_G and G/λ. Note that, as expected, T becomes independent of B as $\tau_G \to 0$ (*i.e.*, as the gaps become fully transparent), while τ_n becomes independent of B as the wakes disappear and $G/\lambda \to 1$. These limits correspond to the idealized cases of a ring composed of flat, opaque wakes alternating with empty gaps on the one hand and a classical, many-particle-thick ring on the other. If $\tau_G \to \infty$ or $G/\lambda \to 0$, the ring becomes opaque at all opening angles (*i.e.*, $T \to 0$).

It might be questioned whether the dependence of T_G on opening angle is indeed given by the classical exponential expression in Eq. (6), which applies to a many-particle-thick, low density ring. We test this hypothesis below by comparing the predicted and observed values of τ_n at a third, intermediate value of B.

3. Observations

The specific occultations discussed here were all obtained with Cassini's Visual and Infrared Mapping Spectrometer (VIMS). This is a flexible instrument that can operate in a number of different modes (Brown et al., 2004). The data discussed here were all obtained in occultation mode, where the imaging capabilities of the instrument are disabled, the short-wavelength VIS channel is turned off and the IR channel obtains a continuous series of 0.8–5.1 μm spectra from a single pixel targeted at the star. To reduce data volume, the normal spectral resolution of the instrument is usually reduced by a factor of eight to $\Delta\lambda \simeq 0.14$ μm, with the spacecraft returning simultaneous time series for 31 spectral channels.

In this mode, a precise time stamp is appended to every spectrum to facilitate reconstruction of the occultation geometry. The available SPICE kernels provided by the Cassini navigation team were used to predict the apparent position of the star in Saturn's ring plane as a function of time. This estimate of the occultation geometry was confirmed to be accurate to within a few kilometers using the known radii of gap edges in the Cassini Division and the outer A Ring (Features 1, 3, 4, 13, 16 and 20 of French et al., 1993).

The goal of this study is to explore how the ring transmission varies with ring opening angle B. However, the general transmission function in Eq. (5) depends not only on B but also on the azimuthal angle, ϕ. Dramatic azimuthal variations in the transmission of the A ring at a fixed B are illustrated in Fig. 2 of Hedman et al. (2007). Strong azimuthal variations can also be seen in the B ring by comparing the ingress and egress cuts across the inner B ring derived from the occultation of CW Leo on Cassini rev 31. Fig. 2 shows that the transmission in the egress profile, where $\phi \simeq 255^\circ$ (*i.e.*, $\theta = 5^\circ$), is systematically greater than that in the ingress profile, where $\phi \simeq 300^\circ$ ($\theta = 50^\circ$). This is consistent with the reports by French et al. (2007) and Colwell et al. (2007) that azimuthal asymmetries are not confined to the A ring, but are also significant in the less-opaque inner part of the B ring.

As discussed above, we can avoid the confounding effects of azimuthal variations in the transmission by judiciously selecting occultations where the wakes are seen nearly end-on. Of the 35 ring stellar occultations observed by VIMS as of 1 July 2008 (the end of Cassini's Prime Mission), we have selected three obtained in late 2006 for the present study: α Scorpii on rev 29, CW Leonis on rev 31 and α Aurigae on rev 34. These three occultations were chosen because in each case the line-of-sight through the rings

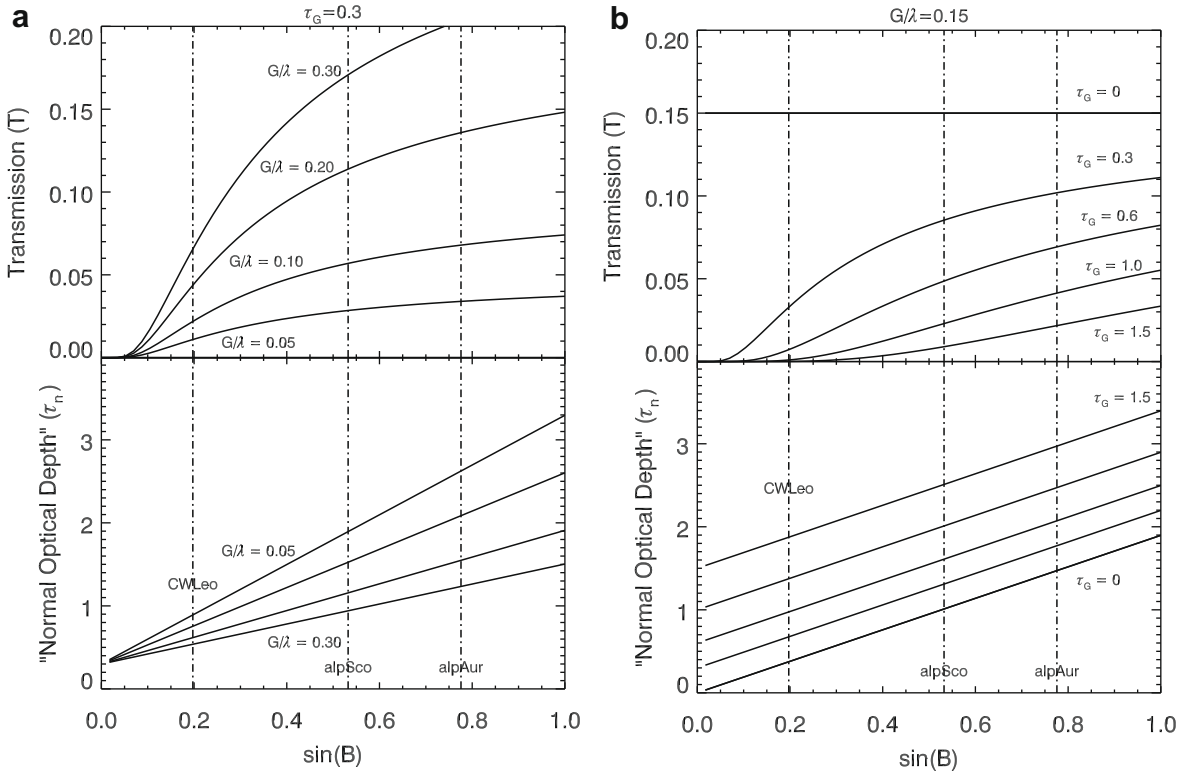

Fig. 1. Model variations of ring transmission and normal optical depth, τ_n, as functions of $\sin B$, for observations where the line of sight is parallel to the self-gravity wakes, based on Eq. (7). Vertical dot-dashed lines correspond to the incidence angles for the stellar occultations of CW Leo, α Sco, and α Aur. Panel (a) shows models for $\tau_G = 0.3$ and values of the gap fraction, G/λ, between 0.05 and 0.30. Panel (b) shows models for $G/\lambda = 0.15$ and values of the gap optical depth, τ_G, between 0.0 and 1.5.

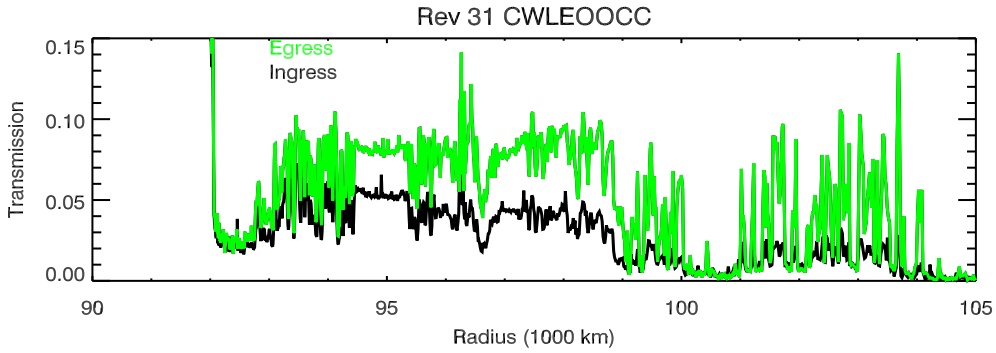

Fig. 2. Ingress and egress transmission profiles of the inner B ring from the occultation by CW Leo on rev 31. The data have been rebinned onto a uniform 5 km radius scale. Note the difference in transmission between the egress profile, which cut the ring at an azimuth, $\phi \simeq 255^\circ$, and the ingress profile for which $\phi \simeq 300^\circ$. The self-gravity wakes are seen end on at $\phi = 70^\circ$ and $\phi = 250^\circ$.

to the star is nearly aligned with the expected orientation of the self-gravity wakes, as shown in Fig. 3. If we assume that the transmission variation with longitude at a fixed value of B has a quasi-sinusoidal shape consistent with Eq. (5) above, then the observed transmission for these three occultations should be within 10% of the peak value, and should therefore provide a reasonably accurate estimate of the maximum transmission of the rings at the relevant ring opening angle.

Table 1 lists several parameters for each occultation used here, including the ring opening angle, B (fixed by the position of the star and Saturn's pole direction), the projected diameter of the stellar disk at the rings, the sampling interval and the radial coverage of the observation. In particular, note that these three stars span a range of $|B|$ from 11.4° (CW Leo) to 50.9° (α Aur), and that each occultation provides almost a full cut across both A and B rings. The radial resolution of the derived optical depth profiles varies from 200 m for α Sco to 3 km for CW Leo, although we note that since the latter's track reaches a minimum radius its resolution is variable. In each case, this resolution is determined by the sampling interval of the data, as this is greater than the projected stellar diameter and/or Fresnel zone (see Table 1).

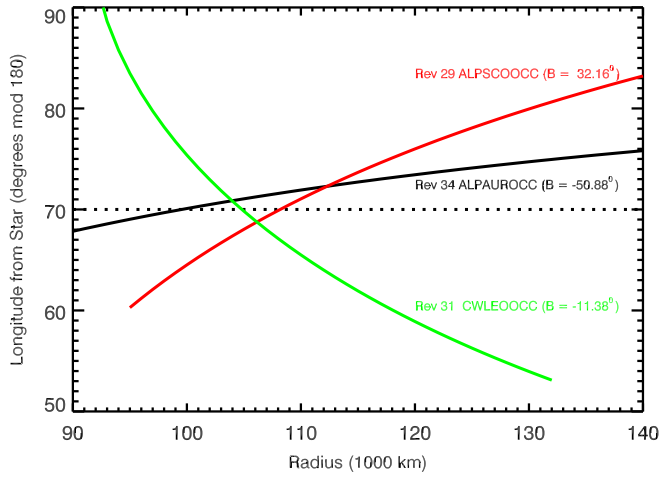

Fig. 3. Variations of the azimuthal angle, ϕ along the ingress tracks for the α Sco and α Aur occultations on revs 29 and 34, and along the egress track for the CW Leo occultation on rev 31. The self-gravity wakes are seen end on at $\phi = 70^\circ$ and $\phi = 250^\circ$, so the azimuths are plotted modulo 180°. The radial range shown spans the A and B rings, for which data are analyzed here; note that the CW Leo egress data end at 132,300 km.

4. Data reduction

The data used in this analysis are uncalibrated,[3] but a mean instrumental thermal background has been subtracted from the spectra. To convert these raw data into estimates of the transmission through the ring T, we must remove background signals due to ringshine and normalize the measured signals from the star.

The signal measured by the VIMS instrument is in general a combination of transmitted starlight and sunlight reflected or diffusely-transmitted by the rings. (In some geometries, the latter can include a significant component of reflected saturnshine, but for present purposes we can lump this together with the reflected sunlight.) We use data from multiple spectral channels to isolate the signal from the star. The channels we consider here correspond to wavelength ranges of 1.01–1.13, 2.87–2.98 and 4.87—4.99 μm, which henceforth we shall refer to as the 1 μm, 3 μm, and 5 μm channels, respectively. The scattered light from the rings is comparatively strong at 1 μm but much less so at 3 or 5 μm, where water ice is strongly absorbing (Nicholson et al., 2008a,b). So the 3 μm and 5 μm channels in general provide much cleaner measurements of the stellar transmission by the rings. However, even these longer-wavelength channels can still exhibit some residual scattered signal from the rings, especially in the most opaque parts of the B ring. The data from the 1 μm channel is thus used to trace the changes in ring background signal with time (or radius), which can then be removed from the longer-wavelength data. Note that because the time variations in the ring background are limited by the *spatial* resolution of the instrument, while the time variations in the stellar signal are limited by the *temporal* resolution, the ring background varies slowly with time compared to the variations in the stellar signal.

Since VIMS stellar occultation data are obtained by measuring the flux in a single rectangular pixel 0.25 × 0.50 mrad in size, the photometric stability of these measurements is limited by the pointing stability of the Cassini spacecraft, and by how well the star is initially centered in the pixel. (The point-spread function of the VIMS IR channel varies with wavelength from ~0.05 to ~0.20 mrad in diameter, and is somewhat smaller than the pixel size.) Spacecraft pointing variations are typically of order 50 μrad once any initial transients damp out, and in many cases the measured stellar signal varies by only a few per cent between the start and end of the occultation, but in other cases we see variations of 5–10%, or occasionally even greater. In such cases it is necessary to

[3] The standard VIMS calibration pipeline converts raw data numbers to spectral reflectivity, I/F, and removes cosmic ray hits via median filtering in the spatial/spectral domain, neither of which procedures is applicable to one-dimensional occultation data.

Table 1
Stellar occultation parameters.

Star	Spec. type	Rev.	Date (yyyy–ddd)	B[a] (deg)	D[b] (m)	δt[c] (ms)	Count rate[d] (DN/s)	Ring coverage
α Sco	M1 Iab	29	2006–269	32.16°	105	20	36,000	A and B[e]
CW Leo	C6	31	2006–301	−11.38°	560	80	1600	A and B[f]
α Aur	G8	34	2006–336	−50.88°	48	80	5200	A, B and C

[a] Ring opening angle. Negative sign indicates view of sunlit rings.
[b] Stellar diameter, projected at the distance of the rings, or Fresnel zone diameter at a wavelength of 3.0 μm, whichever is larger.
[c] Sampling interval.
[d] Unocculted stellar flux at 2.9 μm (at 4.9 μm for CW Leo).
[e] Minimum radius of 94,700 km in the inner B ring.
[f] Track turned around at 91,400 km in the outer C ring.

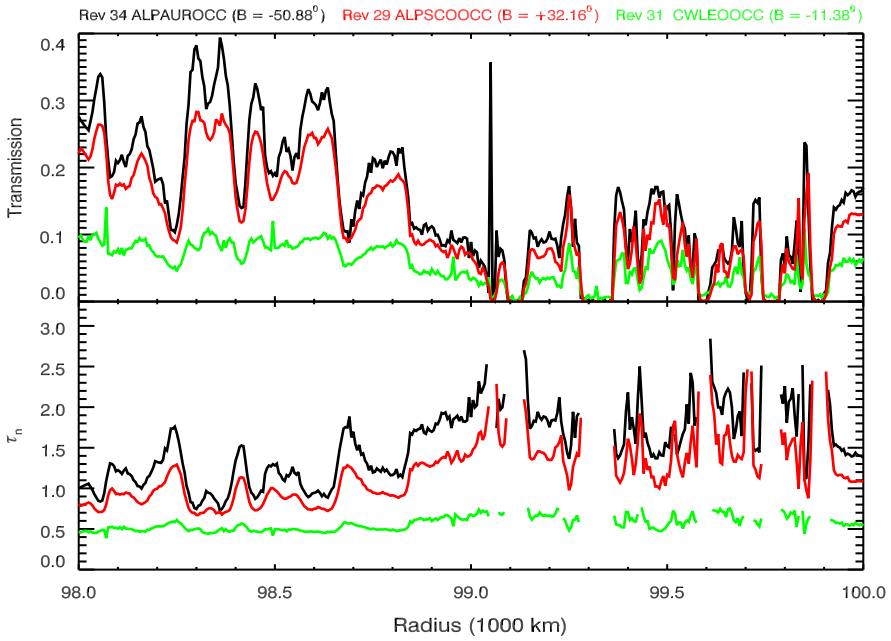

Fig. 4. Radial profiles of transmission (top) and normal optical depth (bottom) for the inner B ring derived from the α Aur, α Sco and CW Leo occultations on revs 34, 29 and 31, respectively. The radial range shown spans the boundary between the B1 and B2 regions at 99,000 km. Note that both T and τ_n (as calculated using Eq. (4)), increase monotonically with the ring opening angle, $|B|$. The optical depths have been suppressed where the transmission drops below 0.01, corresponding to $\tau_n = 2.4$ at $B = 32°$. Narrow spikes at 98,070, 98,500, 98,950 and 99,050 km are due to cosmic ray hits.

estimate a time-dependent correction to the stellar baseline flux and remove this trend from the raw data. (Unfortunately it does not appear possible to correct for such pointing variations using data from additional spectral channels, as all channels suffer approximately the same effects.)

The level of background ringshine and the amount of drift in the observed stellar flux varies significantly from occultation to occultation, so it is not possible to define a single generic procedure for converting the raw data to transmission estimates. Instead, slightly different methods are used for each of the different data sets considered here. The interested reader is referred to Appendix A for a more detailed discussion.

5. Results

Even a cursory comparison of the optical depth profiles derived from the three occultations reveals the shortcomings of Eq. (3). In Fig. 4 we compare normalized transmission and optical depth profiles for a representative region in the inner B ring, where τ_n is computed from the transmission profiles using Eq. (4) above. In agreement with Colwell et al. (2007), we find that τ_n increases monotonically with $|B|$. The most marked difference occurs between 11.4° and 32.2°, with only a modest (∼20%) further increase between 32.2° and 50.9°. As noted by Colwell et al., the fact that *any* appreciable light is transmitted through the B ring at inclination angles as low as 11° can only be accounted for by the presence of virtually empty gaps. As an example, we note that if the transmission of ∼0.10 measured at $B = 51°$ at a radius of 99,000 km were scaled following Eq. (3), then we would expect that $T \simeq 1.2 \times 10^{-4}$ in the CW Leo data, 300 times less than the observed value of ∼0.04.

However, while the B ring evidently does not conform to the classical behaviour enshrined in Eq. (3), neither is the transmission independent of B, as expected for a pattern of opaque wakes, viewed end-on and separated by completely empty gaps. In fact, the transmission at 11.4° is only one-third to one-half of that at 50.9° in this region.[4] Evidently, the true situation is somewhere in between these two idealized models, with the simplest interpretation being that the 'gaps' between the wakes are filled with partially-transparent material. In fact, it turns out that we can account for the observed variation of τ_n with B at almost all locations in the A and B rings using Eq. (7) with an appropriate combination of fractional gap width, G/λ, and optical depth, τ_G.

[4] This is at variance with the statement by Colwell et al. (2007) on page 137 that "at virtually all locations in the B ring, [the transmission] is roughly independent of B."

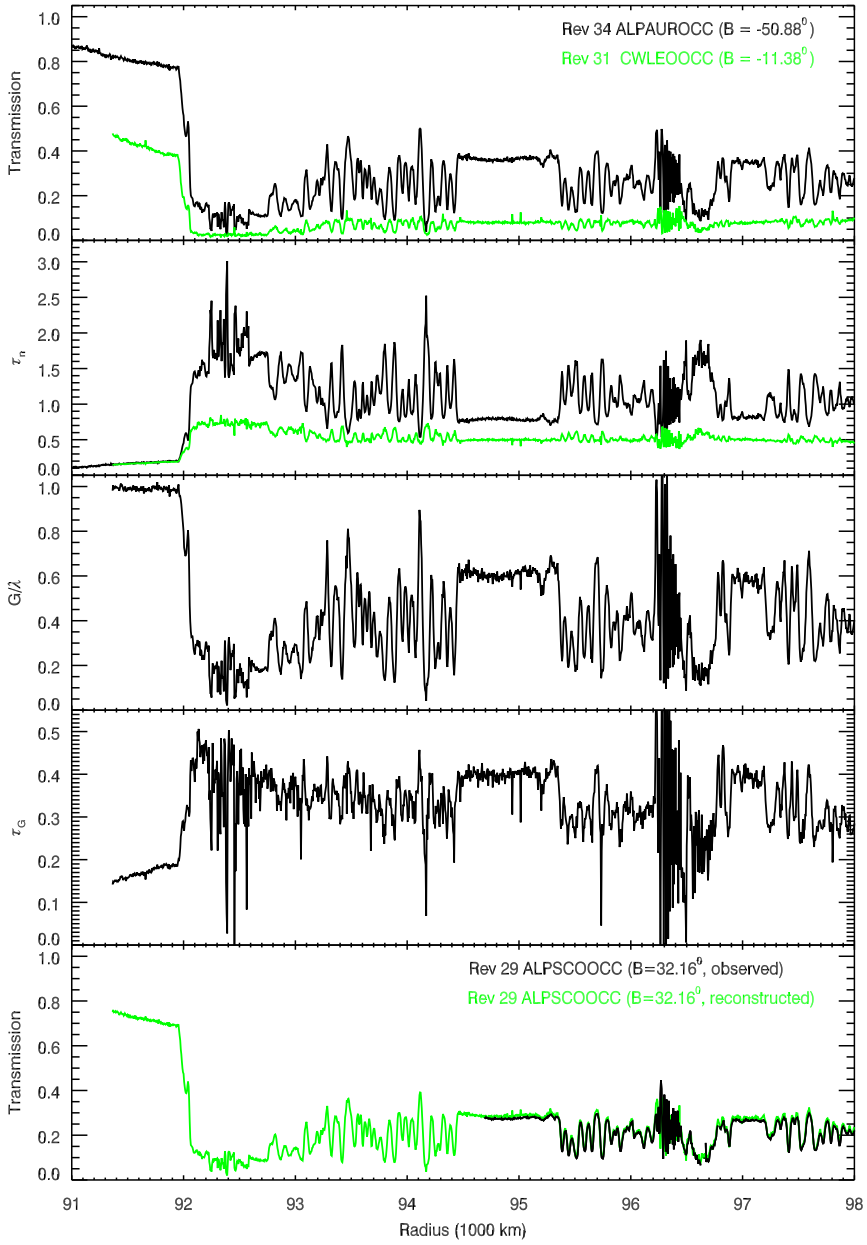

Fig. 5. The first and second panels show radial profiles of transmission and normal optical depth for the inner B ring derived from the α Aur and CW Leo occultations at $B = -50.88^\circ$ and $B = -11.38^\circ$, respectively. The radial range shown spans most of the B1 region (92–99 Mm). The third and fourth panels show the wake model parameters G/λ and τ_G derived from these data using Eq. (7). The fifth panel shows the predicted transmission at $B = 32.16^\circ$ (grey curve) compared with the α Sco ingress profile (black curve), which ends at 94,700 km. The 'noisy' region at 96,300 km is due to the strong Janus 2:1 density wave.

The CW Leo ($B = -11.23^\circ$) egress and α Aur ($B = -50.88^\circ$) ingress occultations provide our largest spread in $|B|$ and we therefore use these two data sets to derive estimates of τ_G and G/λ from Eq. (7). Figs. 5–9 show the results of these calculations. In each of these figures, the top panel shows the transmission curves for these two occultations, which have either been rebinned (α Aur) or interpolated (CW Leo) onto a regular 5 km array of radii to facilitate the calculations. The second panel shows the computed value of τ_n for each data set, from Eq. (4), while the third and fourth panels show the values of τ_G and G/λ derived from fitting Eq. (7) to these data. Finally, the bottom panel shows the predicted transmission at an intermediate value of $B = 32.16^\circ$ for these same parameters, compared with the observed transmission curve for the α Sco occultation (also rebinned onto the same 5 km array of radii). This provides a test of the model parameters and of the consistency among the three data sets.

5.1. The B ring

Our first three figures cover the B ring, corresponding roughly to the regions B1, B2 and B4 defined by Marouf et al. (2006a) in their preliminary study of Cassini radio occultation data.[5] Except for the innermost 700 km, the B1 region in Fig. 5 is only moderately opaque and we have good signals from both stars at all radii less than 99,000 km. Throughout this region, we find a relatively uniform value of τ_G, ranging from a minimum of 0.25 to a maximum of 0.40. The fractional gap widths, on the other hand, vary from as little as 0.2 to a maximum of 0.6, with a few outliers as low as 0.1 or high as 0.8, and closely track the regular undulations in τ_n. (The anoma-

[5] In the B3 region, or "core" of the B ring – between radii of 104,000 and 110,000 km – the transmission in the CW Leo data is too low for application of our procedure.

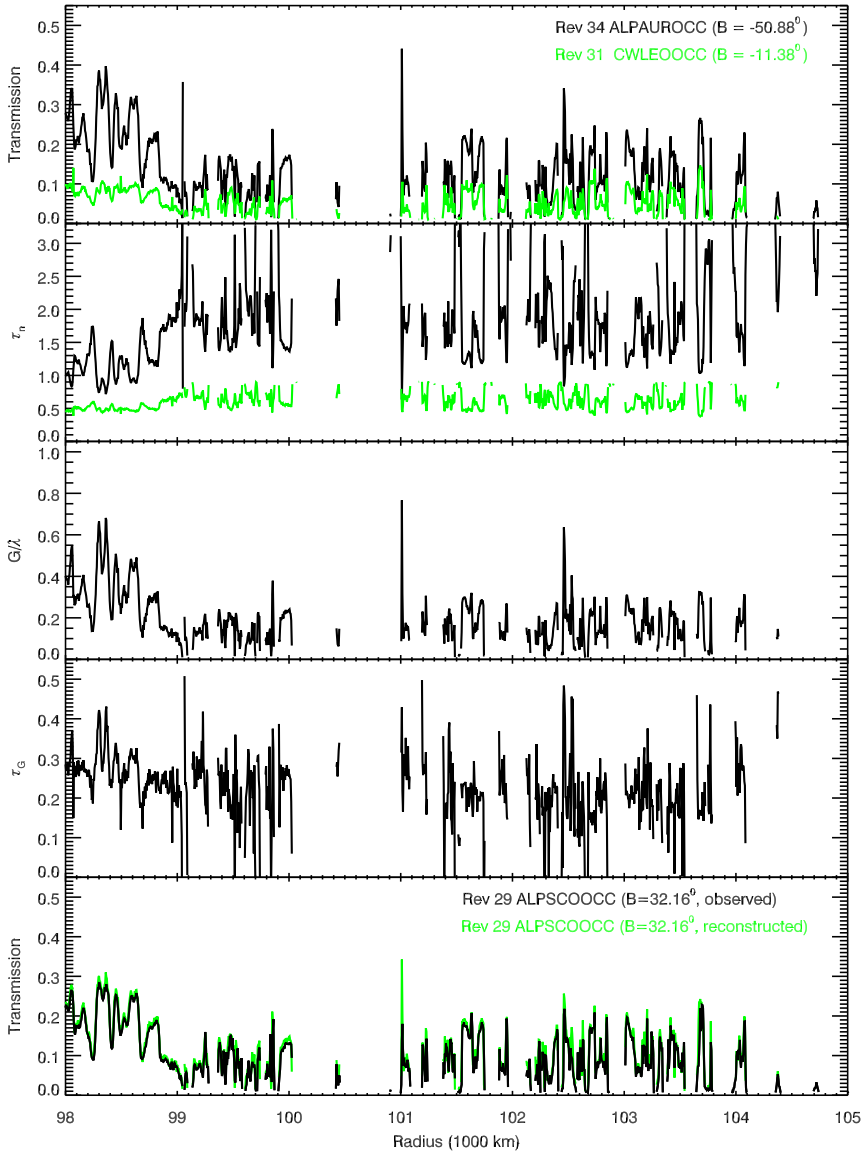

Fig. 6. As in Fig. 5, but for the B2 region (99–104 Mm). The occultation and model parameter profiles have been suppressed where the transmission drops below 0.01, corresponding to $\tau_n = 2.4$ at $B = 32°$; no meaningful fits can be obtained in this regime. In this region, the predicted and observed transmissions at $B = 32.16°$ in the bottom panel are almost indistinguishable.

lously noisy region centered at 96,300 km is due to the strong Janus 2:1 density wave, whose individual crests and troughs do not line up between the CW Leo and α Aur occultations, resulting in a large scatter in the derived values of τ_G and G/λ.) Outside 94,700 km, the measured transmission in the α Sco occultation is in excellent agreement with that predicted by our model parameters.

Between radii of 99,000 and 104,000 km, in the region designated B2 by Marouf et al. (2006a), the character of the ring's radial profile changes to an alternating pattern of low and high optical depth zones, with a characteristic radial scale of 100–200 km (Fig. 6). In the more opaque zones, where $\tau_n > 3$, the CW Leo data are saturated and we cannot estimate τ_G or G/λ. But in the less opaque zones we obtain quite well-defined values: τ_G falls primarily in the range 0.15–0.30, not greatly different from that in B1, while G/λ ranges from 0.1 to 0.3. As in B1, the largest fractional variation is seen in the gap widths. Note that the region between 100,000 and 101,000 km is almost completely opaque, with only a very small 'window' at ~100,450 km. As in region B1, the measured transmission in the α Sco occultation is in excellent agreement with that predicted by our model parameters.

Outside 110,000 km, in the region known as B4, we again have adequate signal at most radii from both α Aur and CW Leo, but the latter data are much noisier than in B1 and B2. In Fig.7 we plot our model parameters binned to a resolution of 20 km in order to reduce the noise level. Here we find that τ_G is again similar to that in the inner B ring, ranging from 0.25 to 0.45, but that the gaps between the wakes are significantly narrower, with G/λ less than 0.20 almost everywhere interior to 117,000 km. While the structure here appears less organized than that in regions B1 or B2, it again seems that fractional variations in gap width, G/λ, are much larger than those in τ_G.

In the outermost 1000 km of the B ring, beyond 116,500 km, the average optical depths drop rapidly with a concommitant increase in G/λ to values as high as 0.7. There is an increasing scatter in τ_G in this region, which may largely reflect that fact that the optical depth profiles show significant azimuthal and/or temporal variations in this

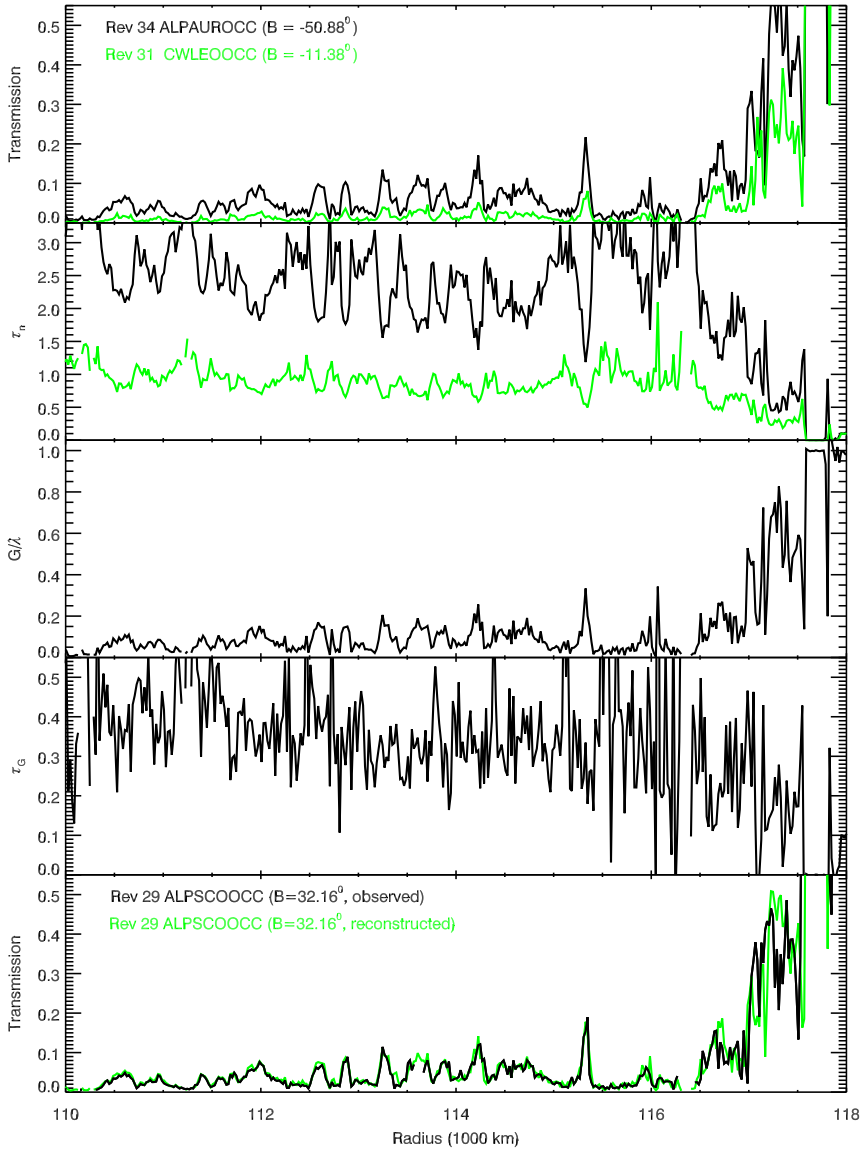

Fig. 7. As in Fig. 5, but for the B4 region (110–117.5 Mm), where the average optical depth is ∼2.0. In order to reduce scatter in the model parameters, the measured profiles were first rebinned to a resolution of 20 km. The occultation and model parameter profiles have been suppressed where the transmission drops below 0.01, corresponding to $\tau_n = 2.4$ at $B = 32°$. Except in the perturbed region beyond 117,000 km, the predicted and observed transmissions at $B = 32.16°$ in the bottom panel are again almost indistinguishable.

region, which is strongly-perturbed by the Mimas 2:1 inner Lindblad resonance (Porco et al., 1984). We therefore consider our estimates of τ_G and G/λ in this region to be questionable.

5.2. The Cassini Division

In the Cassini Division a very different picture presents itself from that in the B ring. In the second panel of Fig. 8, we see that both α Aur and CW Leo occultations yield almost identical estimates of the normal optical depth, τ_n. According to Eq. (7), therefore, $G/\lambda \simeq 1.0$ and virtually all of the observed variation in τ_n must be due to variation in τ_G. In other words, there appear to be virtually no self-gravity wakes in this region and the transmission is well-described by the classical expression, Eq. (3). The most prominent exceptions to this generalization are found in the unique 'triple band' feature at 120,500–120,800 km and in the narrow ringlet at 120,100 km, where G/λ drops below 0.8. We also note that there is a small but steady decrease in G/λ across the ramp which terminates the Cassini Division.

As in the B ring, the α Sco data in the lower panel are again consistent with the transmission predicted by our simple model.

5.3. The A ring

As expected, the self-gravity wakes reappear in the inner A ring, as seen quite dramatically in Fig. 8. The transition at a radius of 122,000 km is very abrupt, with G/λ decreasing from 0.95 to ∼0.3 in a distance of only 300 km. In the inner A ring, between 122,000 and 126,000 km, τ_G decreases slowly but irregularly from ∼0.30 to 0.14. Over this same range the gaps widen, with G/λ increasing from ∼0.30 to a high of 0.60. Local bursts of 'noise' are again due to strong spiral density waves, where the crests and troughs do not align between the two occultations. The most notable is the Janus/Epimetheus 4:3 wave at 125,300 km.

In the middle A ring, defined here as the radial range 126,000–130,000 km, τ_G is almost constant at ∼0.15 while G/λ increases slowly from 0.55 to 0.65 (Fig. 9). Numerous density waves due to Pandora and Prometheus provide the only small-scale structure.

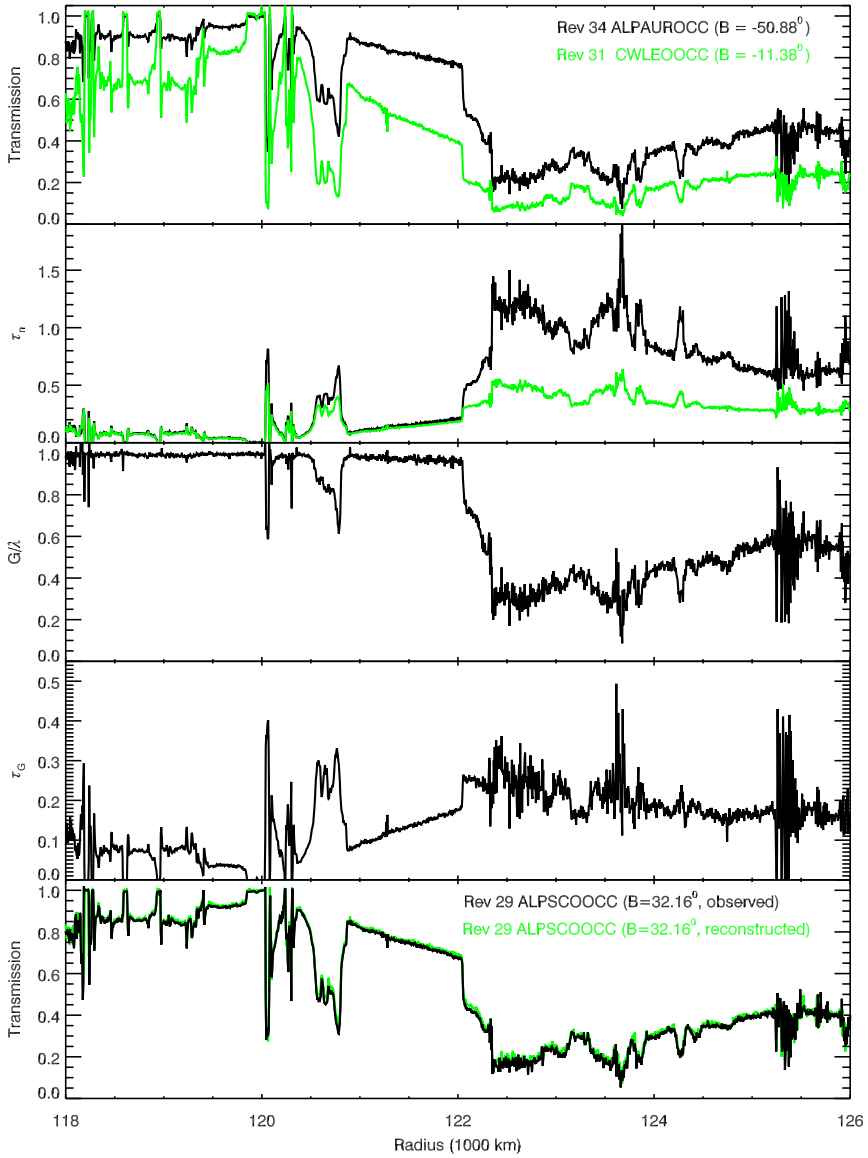

Fig. 8. As in Fig. 5, but for the Cassini Division (118–122 Mm) and inner A ring. Self-gravity wakes appear to be absent, or extremely weak, in the Cassini Division, except for the narrow, dense ringlet at 120,100 km and the 'triple band' at 120,700 km. The 'noisy' region at 125,300 km is due to the strong Janus 4:3 density wave. In both the Cassini Division and inner A ring, the predicted and observed transmissions at $B = 32.16°$ in the bottom panel are again almost indistinguishable.

In both the inner and middle A ring the α Sco data are again quite consistent with the transmission predicted by the self-gravity-wake model.

The CW Leo data stop at 132,300 km, before reaching the outermost parts of the A ring, so to cover this region we repeat our calculations using instead the peak transmissions derived for the A ring from the *o* Ceti occultations by Hedman et al. (2007), at $B = -3.45°$. These results are shown in Fig. 10, where again the bottom panel compares the predicted transmission at $B = 32.16°$ with data from the α Sco occultation. The lower noise level here in comparison with that in Fig. 9 reflects the fact that the *o* Ceti transmission profile was binned to 20 km resolution (Hedman et al., 2007). Where they overlap, the estimates of wake parameters are quite consistent with those in Fig. 9: τ_G increases slowly from a minimum of 0.12 at ~129,000 km to 0.18 at the Encke gap, and then to 0.24 at the outer edge of the A ring at 136,700 km. At the same time, G/λ remains fairly constant at 0.65 ± 0.05.

Particularly notable in this region are several strong density waves — the Janus/Epimetheus 5:4 and 6:5 waves at 130,700 km and 134,300 km, respectively, as well as the Mimas 5:3 density wave at 132,400 km — together with the Mimas 5:3 bending wave at 131,800 km. Within ~300 km on either side of each density wave is a region in which τ_G is elevated by a few percent relative to the general background level. These features are coincident with the density wave "halos" seen in VIMS near-infrared spectra of the A ring, where the water-ice band depths are reduced with respect to neighboring regions (see Nicholson et al., 2008a; Fig. 28). Note that the halos extend much further than the actual wavetrains, whose effect on the transmission profile at our resolution of 5 km is noticeable only over ~200 km. Although IR band depths seem to be unaffected by the Mimas bending wave, there is a strong drop in G/λ centered on this feature. As this feature involves vertical distortions, the implications of this drop are unclear.

Although there appears to be a small but systematic difference between the α Sco data and the transmission predicted by our wake model in the region outside the Encke Gap in Fig. 10, this might easily be due to a systematic error in the (very low) *o* Ceti fluxes in this region.

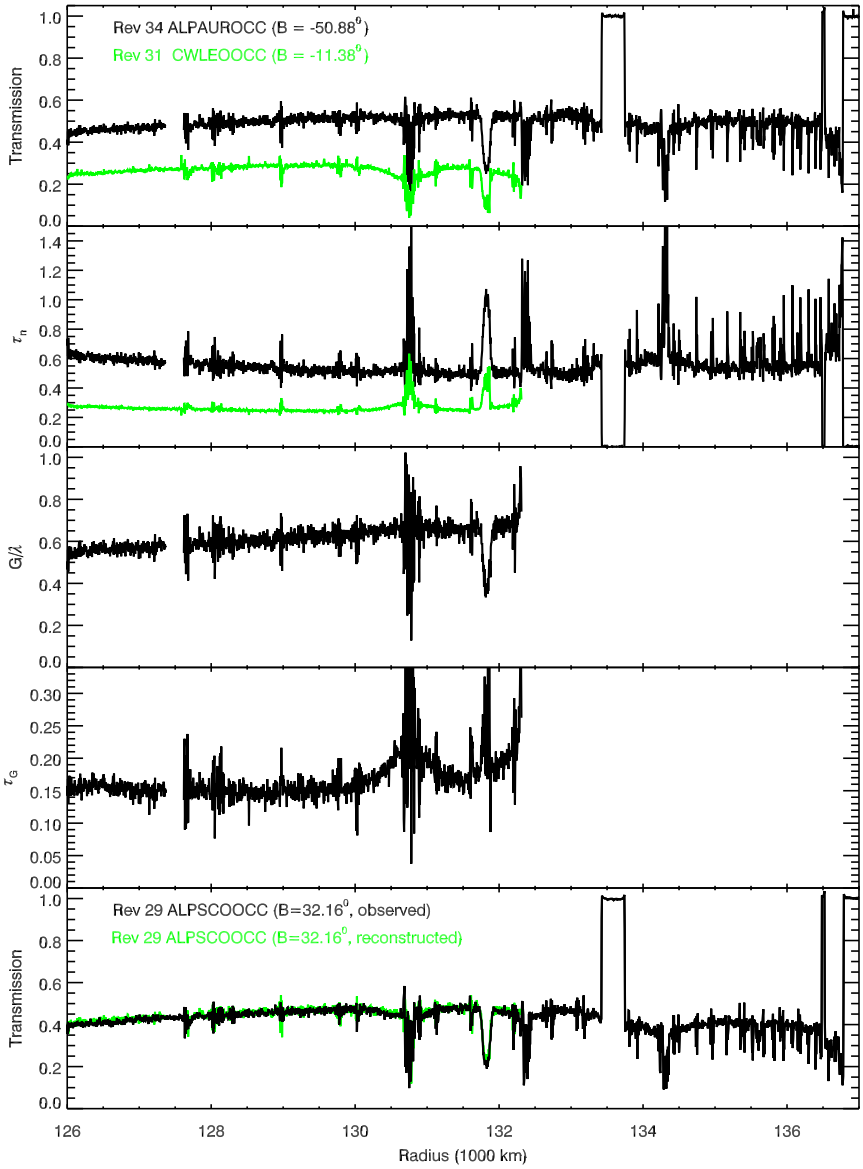

Fig. 9. As in Fig. 5, but for the middle A ring. The CW Leo egress data end at 132,300 km, so wake parameters cannot be computed outside this radius. The 'noisy' region at 130,700 km is due to the Janus 5:4 density wave, on either side of which we see a prominent 'halo' where τ_G is enhanced. As in both the B ring and the Cassini Division, the predicted and observed transmissions at $B = 32.16°$ in the bottom panel are again almost indistinguishable.

6. Discussion

Although it is based on a rather idealized geometric picture of the self-gravity wakes, we find that our simple two-parameter analytical model for the maximum transmission of the rings as a function of opening angle, Eq. (7), provides an excellent fit to data from our three stellar occultations. The predicted transmission at $B = 32.2°$, based on measurements at $|B| = 11.4°$ and at 50.9°, is almost indistinguishable from that measured in the α Sco occultation, suggesting that our assumption of classical, exponential scaling for T_G cannot be too far from the truth. An additional test is provided by the middle A ring, where Figs. 9 and 10 present estimates of τ_G and G/λ based on measurements at $|B| = 11.4°$ for CW Leo and 3.5° for o Cet. The close agreement found here between quasi-independent estimates provides further support for our assumed scaling of T_G with $\sin|B|$.

Our results provide additional strong support for the emerging theoretical paradigm (Daisaka and Ida, 1999; Salo, 1995; Salo and Karjalainen, 2003; Robbins et al., 2008) that the microstructure of the dense A and B rings, and thus their light scattering and emissivity behaviour, are dominated by self-gravity wakes. Together with other recent observations at ultraviolet, visible, mid-infrared and microwave wavelengths (Dunn et al., 2004; Nicholson et al., 2005; Colwell et al., 2007; French et al., 2007; Hedman et al., 2007; Ferrari et al., 2009), our results can be used to test and refine numerical models of the rings, leading ultimately to improved knowledge of both the collisional properties and size distribution of the ring particles in various regions. Preliminary work in this direction has been done by Porco et al. (2008), utilizing *Cassini* images.

Our detailed results presented in Figs. 5–10 above in the form of radial plots of the wake parameters G/λ and τ_G, are summarized in Table 2. Particularly striking is the result that, with the exception of the Cassini Division where wakes appear to be largely absent or at least very weakly-developed, most of the observed variations in normal optical depth, τ_n are due to variations in the gap fraction, G/λ. This parameter may be interpreted, more generally, as the fractional area of the rings which is *not* occupied by dense

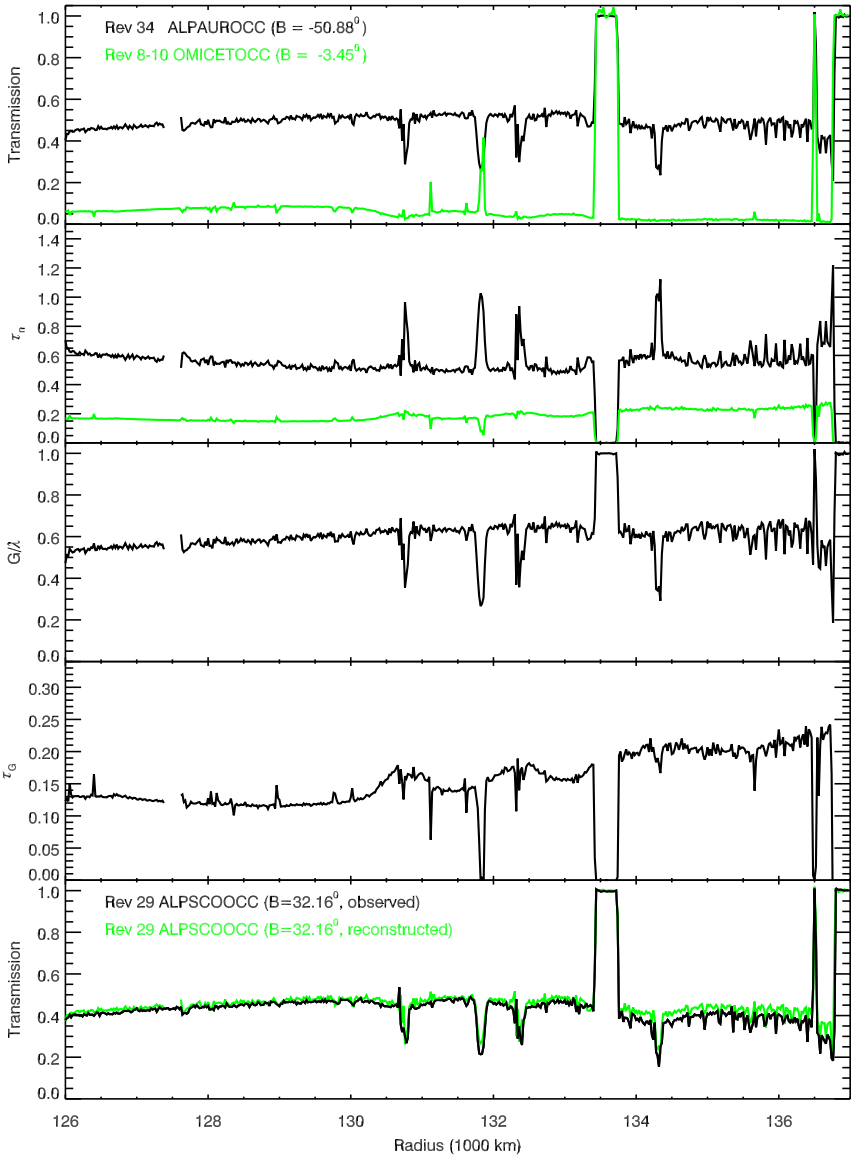

Fig. 10. As in Fig. 9, but for the outer A ring. For this plot we estimate the wake parameters from a combination of the α Aur data at $B = -50.88^\circ$ and the maximum transmission obtained by Hedman et al. (2007) from the o Cet occultations at $B = -3.45^\circ$, which were binned to a resolution of 20 km. Note the 'halos' on either side of the Janus 5:4 and Mimas 5:3 density waves at 130,700 and 132,400 km, where τ_G is enhanced. The prominent dip in transmission, G/λ and τ_G at 131,800 km is due to the Mimas 5:3 bending wave, which has no halo. Again, the predicted and observed transmissions at $B = 32.16^\circ$ in the bottom panel are in good agreement, though with some divergence outside the Encke Gap.

self-gravity wakes. We find that the average value of G/λ varies from as little as 0.05 in parts of the outer B ring to 0.7 in the outermost parts of the A ring. Even within subunits of the B ring (*e.g.*, regions B1 and B2), G/λ varies by a factor of three on scales of only several hundred kilometers.

In contrast to this extreme variability in gap fraction, we find that the optical depth of the regions between the optically-thick wakes, τ_G is much more homogeneous. Across the A ring, τ_G ranges from 0.12 to 0.30, but these variations are mostly smooth, with large changes occurring on scales of thousands of kilometers. Even in the B ring, where the observed optical depths are much more variable on all scales than they are in the A ring, τ_G only varies between 0.15 and $\sim$0.45. In any given subregion, the variation is at most a factor of two. These variations again appear to be rather smooth, except in the undulating structure in region B1 where there are local oscillations in τ_G which track the larger variations in G/λ.

Only in the middle and outer A ring do we find a larger fractional variation in τ_G than in G/λ, and this is largely associated with the presence of several strong density waves (see further discussion below).

A more quantitative way to express the above results is to calculate the linear correlation coefficient between the observed optical depth, τ_n and the wake parameters in various regions. In the last two columns of Table 2 we list the results of such an exercise, where for the true normal optical depth we use the value of τ_n calculated from our wake model parameters at $B = 90^\circ$. As expected, we find a very high correlation between τ_n and $\ln(G/\lambda)$ ($r \geqslant 0.96$) everywhere in the A and B rings, but not in the Cassini Division. The correlation between τ_n and τ_G, on the other hand, is quite low throughout the A and B rings, but exceeds 0.8 in the Cassini Division. Scatter plots of τ_n vs τ_G and G/λ confirm these conclusions, but provide little additional insight.

Table 2
Self-gravity wake model parameters.

Ring region	radius range (Mm)	G/λ[a]	τ_G[b]	r_1[c]	r_2[d]
B1	93–99	0.20–0.60	0.25–0.40	0.99	–0.50
B2	99–104	0.10–0.30	0.15–0.30	0.99	–0.47
B4	110–116.5	0.05–0.20	0.25–0.45	0.99	0.02
B5	116.5–117.5	0.20–0.70	0.15–0.25		
inner Cass. Div.	118–120	1.00	0.04–0.15	0.52	0.83
outer Cass. Div.	120–122	0.65–1.00	0.05–0.30	0.95	0.93
inner A ring	122.3–126	0.30–0.60	0.15–0.30	0.99	0.29
middle A ring	126–130	0.55–0.65	∼0.15		
outer A ring	130–133.4	∼0.65	0.12–0.18	0.96	0.45
trans–Encke	133.7–136.5	∼0.65	0.19–0.23		
trans–Keeler	136.5–136.7	∼0.55	∼0.24		

[a] Fractional gap width.
[b] Gap optical depth.
[c] Pearson correl. coeff.: τ_n vs $-\ln(G/\lambda)$.
[d] Pearson correl. coeff.: τ_n vs τ_G.

A plausible deduction from the above is that most of the structure we see in the optical depth profiles of the A and B rings reflects not variations in the total amount of ring material per unit area (*a la* Eq. (2)) but variations in the fraction of ring area which is covered by wakes. Although it seems reasonable to assume that the gap fraction is smaller when the total surface mass density is higher, this relationship can be highly nonlinear (Robbins et al., 2008). Since the wakes themselves appear to be effectively opaque, it is difficult to place an upper limit on the amount of material which might be 'concealed' within them (Robbins et al., 2007).

A corollary to the above picture is that the slowly-varying optical depth of the interwake gaps, τ_G may represent not so much a low-density, horizontal 'sandwich filling' between the wakes as a thick, broadly-distributed 'haze' of smaller particles which envelops the wakes (Nicholson et al., 2007, 2008b). This view is supported by numerical simulations by Salo and Karjalainen (2003) which show that the larger (meter-size) ring particles are mostly confined to the self-gravity wakes, whereas the smaller (cm-size) particles are not. Such simulations also predict that the vertical scale height of the larger ring particles is less than that of the smaller ones, so that the tenuous material represented in our simple model by τ_G may in fact extend across both the wakes and the gaps.

Notwithstanding the above generalizations, our model fits also reveal several curious local anomalies which defy the general trends in each region:

(1) In the regular undulations which dominate most of the B1 region, there is a strong positive correlation between G/λ and τ_G, *i.e.*, where the gaps are wider (and the ring less opaque) τ_G is actually *larger*. This rather counter-intuitive result is evident in a close inspection of Fig. 5, but we can offer no obvious explanation.
(2) While for most of the Cassini Division, $G/\lambda \simeq 1.0$ and wakes are absent, very narrow or weakly-developed, they reappear in both the dense, narrow Laplace ringlet at 120,100 km (designated R10 in the review article by Colwell et al. (2009)) and in the 'triple band' centered at 120,700 km (see Fig. 8). This may simply reflect the fact that these are the most opaque regions within the Cassini Division; if so, then it would appear that the critical optical depth for the wakes to "turn on" is around $\tau_n = 0.25$. It is noteworthy that only in the outer Cassini Division do we find significant correlations between τ_n and both G/λ and τ_G.
(3) At both the inner edge of the B ring (Fig. 5) and at the inner edge of the A ring (Fig. 8), in addition to the expected decrease in wake spacing there is an abrupt increase in τ_G. This is most noticeable at the B ring edge, where τ_G goes from 0.20 to 0.45 over a distance of ∼150 km. The smooth 'ramps' in optical depth which precede both of these transitions are characterized by almost constant values of G/λ but steady increases in τ_G. Nicholson et al. (2008a) have also noted smooth variations in visible and near-infrared spectral properties (including water ice band depths) across these two ramps.
(4) As noted above, local variations in wake parameters, especially τ_G, are associated with the strong density and bending waves in the outer A ring (Fig. 10). Within the actual wavetrains, the average τ_n increases significantly. The model fits show that this is primarily due to a decrease in G/λ, *i.e.*, to more closely-spaced wakes, rather than to any increase in τ_G. In fact, we find a modest *decrease* in τ_G in most of the density waves, and a dramatic drop in the Mimas 5:3 bending wave. This is somewhat surprising, as a common interpretation (*e.g.*, Nicholson et al., 2000) of the reduced transmission through strong waves invokes an enhanced population of smaller particles produced by a supposedly-more-vigorous collisional regime as the waves damp. A word of caution is in order here, however, as the phase and therefore the detailed optical depth profile of the waves differ between occultations, which means that the application of Eq. (7) even to rebinned data is a little suspect.
(5) Outside the density wavetrains themselves, we see halos of *increased* τ_G which extend to distances of ∼300 km both inwards and outwards from the resonances. Close inspection of Fig. 10 shows that the halos are seen most clearly in the very low-inclination *o* Ceti data, where they appear as increases in optical depth, and are best-developed for the Janus 5:4 and Mimas 5:3 density waves. In their previous analysis of the *o* Ceti data, Hedman et al. (2007) noted that these regions were also associated with a shift of ∼3° in the orientation of the wakes, which they attributed to a decrease in mean particle size. Similar density wave 'halos' were first reported by Dones et al. (1993) in Voyager imaging data and subsequently by Nicholson et al. (2008a) in the water ice band depths derived from high-resolution VIMS spectral scans of the A ring (see their Figs. 18 and 28). Dones et al. noted that the halos are characterized by a more backscattering phase function than the average in the A ring (see their Fig. 14), while Nicholson et al. attributed the near-IR halos to local decreases in either regolith grain size or ice purity. As they extend both interior and exterior to the density waves, the halos cannot be directly attributed to the effects of wave collisional damping; it is possible, however, that ballistic transport (Durisen et al., 1989) is acting to redistribute small collisional debris over a broader zone than the waves themselves. Although a clear picture of their underlying nature has not yet emerged, it is clear that the halos are regions of particular interest in the A ring.

Finally, we compare our estimates of the self-gravity wake parameters with those of Colwell et al. (2006) for the A ring and Colwell et al. (2007) for the B ring. These authors employ a very similar model for the wakes, except that the wake cross-section is assumed to be rectangular ($W \times H$) rather than elliptical. Noting that their wake spacing, $S \simeq G$ in our model, we have $G/\lambda = S/(S+W) = S/W/(S/W+1)$.

For the A ring, Colwell et al. (2006) present plots showing the variations of τ_G and the ratio H/W with radius (see their Fig. 4). They find that τ_G increases from a minimum of 0.12 at around 129,000 km to 0.24 outside the Encke Gap, in excellent agreement with our results in Figs. 9 and 10. Over most of the A ring, they find that S/W increases smoothly from 1.35 to 2.85, or $G/\lambda = 0.58$ to

0.74 which is also in good agreement with our results. Both studies find that G/λ is significantly smaller in the inner 2500 km of the A ring, although Colwell et al.'s estimate of 0.50 is based on only a single measurement at 123,300 km. Our results (Fig. 8) reveal significant variations in G/λ inside of 125,000 km.

In the B ring, Colwell et al. (2007) reach the same principal conclusion as we do: that the effective normal optical depth of the ring is controlled largely by the spacing between the wakes, which they express in terms of the ratio S/W. In their Fig. 17, they show a tight negative correlation between τ_n and S/W. On the other hand, Colwell et al. find that "there are no correlations between τ_G and either position in the ring, total optical depth, or other self-gravity wake parameters." While in general we agree that there is little correlation between τ_G and τ_n in the B ring, we do see large-scale trends with radius in Figs. 5–7, as well as the local correlations with G/λ in region B1 noted above. Our numerical values are in good agreement: using a numerical ray-tracing method, Colwell et al. find $0.15 < \tau_G < 0.30$ in regions B1 and B2, and $0.2 < \tau_G < 0.5$ in region B4.

Acknowledgments

This work was carried out with financial support from NASA via the Cassini-Huygens program. We thank Mike Evans and Matt Tiscareno for providing code that was used to help reconstruct the occultation geometry, and Brad Wallis for updated predictions of the event timings. We also acknowledge many fruitful (and sometimes steamy) discussions with Heikki Salo, who provided access to his as-yet-unpublished models of self-gravity wakes and an insightful review by Essam Marouf which challenged us to reexamine our assumptions. These data would not have been obtained without the contributions of many people on the VIMS Science and Engineering teams, especially Orland Harrison who wrote the onboard occultation software after the spacecraft had been launched.

Appendix A. Photometric reduction of occultation data

A.1. α Aurigae occultation (rev 34)

For the α Aur occultation on Rev 34, we were fortunate in that the path of the star behind the rings as seen by Cassini fell entirely within the part of the rings that was in Saturn's shadow. There is consequently no detectable reflected light from the rings even in the 1 μm channel. Furthermore, the signal measured through the most opaque part of the B ring was well below 0.1% of the unocculted stellar signal, so there is no evidence for any residual instrumental background. Consequently, no subtraction of background ring signal was necessary for this data set. All that was necessary to convert raw data numbers to measurements of ring transmission was to normalize the 3 μm data. This occultation cut through the entire ring system, from F to D rings, so we could determine the mean unocculted stellar signal both outside the F ring (between radii of 142,000 and 143,000 km) and inside the C ring (between 69,000 and 70,000 km). These two values differed by less than 1%, so the star's signal was quite stable for this occultation. We therefore assumed a linear drift in the stellar baseline over time (fitted to the two measured values of the unocculted flux) to normalize the data.

A.2. CW Leonis occultation (rev 31)

For the CW Leo occultation on Rev 31, on the other hand, the star passed behind the fully illuminated rings and significant reflected light can be observed at all wavelengths. The geometry was a "chord occultation", *i.e.*, one in which the apparent track of the star cut more-or-less vertically across one ansa of the rings rather than radially, reaching a minimum radius of ∼91,400 km in the outermost part of the C ring. Observations ended just before the star exited the A ring, at a radius of ∼ 132,300 km. Only the egress segment is of interest here, with $\phi \simeq 250^\circ$ (see Fig. 2).

In this case we exploit the fact that CW Leo (a carbon star also known as IRS 10216, and one of the brightest objects in the IRAS all-sky survey at 12 μm) is an extremely red object which produces no detectable signal in the VIMS data at wavelengths shortward of ∼2 μm. The data from the 1 μm channel therefore provide a direct measure of how the signal from the rings varied over the course of the occultation. Based on data from other occultations, we know that at a ring opening angle of 11° the B ring is essentially opaque between radii of 105,700 and 106,100 km, so that the entire signal seen during the time the star passed behind this part of the rings must be from the rings themselves. We therefore scale the ring brightness profile obtained from the 1 μm data by the ratio of the average signals in this region at 5 μm and 1 μm and subtract this scaled template from the 5 μm data. This removes most of the ring background from these data, which amounts to ∼5% of the unocculted stellar flux.

However, if we compare the background levels during ingress and egress in the region between 105,700 and 106,100 km, we find a residual difference of ∼1% of the unocculted stellar signal. This suggests the above procedure did not completely remove the scattered light from the rings. This may be due to subtle differences in the spectral properties of the rings with longitude due to saturnshine on the rings. More detailed photometric modelling could potentially yield a better background subtraction. However, this residual is so small that we chose instead simply to assume that the background drifts linearly in time over the course of the occultation. We therefore use the two measurements of this level from ingress and egress to determine the slope of the drift and remove it from the data.

Finally, to normalize the stellar flux at 5 μm, we compute the average signal in the Huygens gap (between 117,650 and 117,750 km) on ingress and egress. (While there are some data from outside the A ring on the ingress side of the occultation, the egress data of interest here stop just short of the Encke Gap.) These two numbers differ by ∼5%, implying a small but detectable change in the baseline signal from CW Leo. Again, since the variation is small, we assume that the baseline level drifted linearly in time and use these two measurements to compute the offset and slope and normalize the data.[6]

A.3. α Scorpii occultation (rev 29)

Our third occultation, that of α Sco on Rev 29, spanned the F and A rings and most of the B ring, but was prematurely truncated at 94,700 km just before reaching the C ring. The star was viewed from the northern, unilluminated side of the rings, so the rings themselves were fairly dark and do not dominate the measured signal at any wavelength. However, the signal due to scattered sunlight from the rings is non-zero, even at 3 μm, and needs to be removed in order to obtain accurate measurements of the transmission. Our first step is to normalize the data from both the 1 μm and 3 μm channels in a region outside the F ring (between 142,000 and 143,000 km) where the only signal should be from the star. Since the transmission through the main rings is observed to be independent of wavelength (Harbison et al., 2008), and the rings' reflectance spectrum is, to first order, independent of radius

[6] We do not make use of the unocculted flux level prior to the A ring ingress, which was ∼10% higher than that observed in the Huygens gap but decreased visibly over several minutes.

(Nicholson et al., 2008a; Filacchione et al., 2008a,b), the signal from the star should be the same for these two normalized data sets, while the reflected-light signal from the rings will differ by a constant multiplicative factor. The difference between the two data sets will therefore be proportional to the signal from the rings alone and can serve as a template for the variations in the ring brightness as a function of radius. To scale this template and determine the absolute magnitude of the ring signal in the 3 μm channel, we again assume that a particular region in the B ring (this time between 105,200 and 105,400 km) is effectively opaque so that the only signal we observe here is reflected sunlight. We find that the appropriately scaled ring template is at most 1% of the unocculted signal from the star in the 3 μm channel.

After removing the ring background, we check the stability of the baseline signal from the star by comparing the mean signal in the Huygens gap (between 117,650 and 117,750 km) with the mean signal outside the F ring (between 142,000 and 143,000 km). These two levels differ by 0.8%, implying that the signal from the star was not completely stable. Assuming again that this difference is due to a small linear drift in the baseline over time, we use these two numbers to measure the slope of the drift and refine the normalization of the data.

References

Brown, R.H., and 21 colleagues, 2004. The Cassini visual and infrared mapping spectrometer (VIMS) investigation. Space Sci. Rev. 115, 111–168.

Colombo, G., Goldreich, P., Harris, A.W., 1976. Spiral structure as an explanation for the asymmetric brightness of Saturn's A ring. Nature 264, 344–345.

Colwell, J.E., Esposito, L.W., Sremčević, M., 2006. Self-gravity wakes in Saturn's A ring measured by stellar occultations from Cassini. Geophys. Res. Lett. 33, 7201.

Colwell, J.E., Esposito, L.W., Sremčević, M., Stewart, G.R., McClintock, W.E., 2007. Self-gravity wakes and radial structure of Saturn's B ring. Icarus 190, 127–144.

Colwell, J.E., French, R.G., Marouf, E.A., Murray, C.D., Nicholson, P.D., Tiscareno, M.S., 2009. The structure of Saturn's rings. In: Brown, R.H., Dougherty, M. (Eds.), Saturn after Cassini-Huygens. Kluwer, pp. 375–409.

Daisaka, H., Ida, S., 1999. Spatial structure and coherent motion in dense planetary rings induced by self-gravitational instability. Earth, Planets, and Space 51, 1195–1213.

Dones, L., Porco, C.C., 1989. Spiral density wakes in Saturn's A ring? Bull. Am. Astron. Soc. 21, 929.

Dones, L., Cuzzi, J.N., Showalter, M.R., 1993. Voyager photometry of Saturn's A ring. Icarus 105, 184–215.

Dunn, D.E., Molnar, L.A., Niehof, J.T., de Pater, I., Lissauer, J.J., 2004. Microwave observations of Saturn's rings: anisotropy in directly transmitted and scattered saturnian thermal emission. Icarus 171, 183–198.

Durisen, R.H., Cramer, N.L., Murphy, B.W., Cuzzi, J.N., Mullikin, T.L., Cederbloom, S.E., 1989. Ballistic transport in planetary ring systems due to particle erosion mechanisms. I — Theory, numerical methods, and illustrative examples. Icarus 80, 136–166.

Ferrari, C., Brooks, S., Edgington, S., Leyrat, C., Pilorz, S., Spilker, L., 2009. Structure of self-gravity wakes in Saturn's A ring as measured by Cassini CIRS. Icarus 199, 145–153.

Filacchione, G., and 16 colleagues, 2008a. The diversity of Saturn's main rings: a Cassini-VIMS perspective. Lunar Planet. Inst. Conf. Abstr. 39, 1294.

Filacchione, G., and 12 colleagues, 2008b. The spectral classes of the Saturnian System ices: rings and satellites observations by Cassini-VIMS. AGU Fall Meeting Abstracts A7.

Franklin, F.A., Colombo, G., 1978. On the azimuthal brightness variations of Saturn's rings. Icarus 33, 279–287.

Franklin, F.A., Cook, A.F., Barrey, R.T.F., Roff, C.A., Hunt, G.E., de Rueda, H.B., 1987. Voyager observations of the azimuthal brightness variations in Saturn's rings. Icarus 69, 280–296.

French, R.G., and 17 colleagues, 1993. Geometry of the Saturn system from the 3 July 1989 occultation of 28 Sgr and Voyager observations. Icarus 103, 163–214.

French, R.G., Salo, H., McGhee, C.A., Dones, L., 2007. HST observations of azimuthal asymmetry in Saturn's rings. Icarus 189, 493–522.

Harbison, R.A., Nicholson, P.D., Cassini VIMS Team, 2008. Searching for sub-centimeter particles in Saturn's main rings. AAS/Division of Dynamical Astronomy Meeting 39, #16.05.

Hedman, M.M., Nicholson, P.D., Salo, H., Wallis, B.D., Buratti, B.J., Baines, K.H., Brown, R.H., Clark, R.N., 2007. Self-gravity wake structures in Saturn's A ring revealed by Cassini VIMS. Astron. J. 133, 2624–2629.

Julian, W.H., Toomre, A., 1966. Non-axisymmetric responses of differentially rotating disks of stars. Astrophys. J. 146, 810–830.

Lumme, K., Irvine, W.M., 1976. Photometry of Saturn's rings. Astron. J. 81, 865–893.

Lumme, K., Esposito, L.W., Irvine, W.M., Baum, W.A., 1977. Azimuthal brightness variations of Saturn's rings. II — observations at an intermediate tilt angle. Astrophys. J. 216, L123–L126.

Lumme, K., Irvine, W.M., 1984. Azimuthal variations in Saturn's A ring. IAU Colloq. 75. Planetary Rings 87–91.

Marouf, E.A., French, R.G., Rappaport, N.J., McGhee, C.A., Wong, K., Thomson, F.S., Anabtawi, A., 2006a. Structure and properties of Saturn's ring B from Cassini radio occultations. Bull. Am. Astron. Soc. 38, 552.

Marouf, E., Rappaport, N., French, R., McGhee, C., Anabtawi, A., 2006b. Azimuthal variability of radial structure of Saturn's rings observed by Cassini radio occultations. 36th COSPAR Scientific Assembly 36, 2806.

Marouf, E.A., French, R.G., Rappaport, N.J., McGhee, C.A., Thomson, F.S., Wong, K., Anabtawi, A., 2007. Cassini radio occultation observations of the structure and properties of Saturn's ring B. EPSC Abstract 2007-A-00094.

Nicholson, P.D., French, R.G., Campbell, D.B., Margot, J.-L., Nolan, M.C., Black, G.J., Salo, H.J., 2005. Radar imaging of Saturn's rings. Icarus 177, 32–62.

Nicholson, P.D., French, R.G., Tollestrup, E., Cuzzi, J.N., Harrington, J., Matthews, K., Perkovic, O., Stover, R.J., 2000. Saturn's rings I. Optical depth profiles from the 28 Sgr occultation. Icarus 145, 474–501.

Nicholson, P.D., Hedman, M.M., Clark, R.N., Brown, R.H., Buratti, B.J., Baines, K.H.Cassini-VIMS Team, 2007. Through a glass darkly: Saturn's enigmatic B ring. Bull. Am. Astron. Soc. 38, 420.

Nicholson, P.D. and 15 colleagues, 2008a. A close look at Saturn's rings with Cassini VIMS. Icarus 193, 182–212.

Nicholson, P.D., Hedman, M.M., Salo, H.J., Cassini VIMS Team, 2008b. Cassini-VIMS observations of self-gravity wakes in Saturn's rings — II. AAS/Division of Dynamical Astronomy Meeting 39, #18.01.

Porco, C., Danielson, G.E., Goldreich, P., Holberg, J.B., Lane, A.L., 1984. Saturn's nonaxisymmetric ring edges at 1.95 R(s) and 2.27 R(s). Icarus 60, 17–28.

Porco, C.C., Weiss, J.W., Richardson, D.C., Dones, L., Quinn, T., Throop, H., 2008. Simulations of the dynamical and light-scattering behavior of Saturn's rings and the derivation of ring particle and disk properties. Astron. J. 136, 2172–2200.

Reitsema, H.J., Beebe, R.F., Smith, B.A., 1976. Azimuthal brightness variations in Saturn's rings. Astron. J. 81, 209–215.

Robbins, S.J., Stewart, G.R., Colwell, J.E., Lewis, M.C., 2007. Simulations of clumping effects in high-optical depth rings. Bull. Am. Astron. Soc. 38, 420.

Robbins, S.J., Stewart, G.R., Colwell, J.E., Lewis, M.C., 2008. Self-gravity wakes in saturnian rings: effects of varying location, particle density, and introducing a particle size distribution. AAS/Division for Planetary Sciences Meeting Abstracts 40, #21.05.

Salo, H., 1992a. Gravitational wakes in Saturn's rings. Nature 359, 619–621.

Salo, H., 1992b. Numerical simulations of dense collisional systems. II — Extended distribution of particle sizes. Icarus 96, 85–106.

Salo, H., 1995. Simulations of dense planetary rings. III. Self-gravitating identical particles. Icarus 117, 287–312.

Salo, H., Karjalainen, R., 2003. Photometric modeling of Saturn's rings. I. Monte Carlo method and the effect of nonzero volume filling factor. Icarus 164, 428–460.

Salo, H., Karjalainen, R., French, R.G., 2004. Photometric modeling of Saturn's rings. II. Azimuthal asymmetry in reflected and transmitted light. Icarus 170, 70–90.

Thompson, W.T., Lumme, K., Irvine, W.M., Baum, W.A., Esposito, L.W., 1981. Saturn's rings — azimuthal variations, phase curves, and radial profiles in four colors. Icarus 46, 187–200.

Tiscareno, M.S., Perrine, R.P., Richardson, D.C., Hedman, M.M., Weiss, J.W., Porco, C.C., Burns, J.A., 2009. An analytic parameterization of self-gravity wakes in Saturn's rings, with application to occultations and propellers. Astron. J., submitted for publication.

Toomre, A., 1964. On the gravitational stability of a disk of stars. Astrophys. J. 139, 1217–1238.

Toomre, A., Kalnajs, A.J., 1991. Spiral chaos in an orbiting patch. In: Sundelius, B. (Ed.), Dynamics of Disc Galaxies. Almquist-Wiksell, pp. 341–358.

Zebker, H.A., Marouf, E.A., Tyler, G.L., 1985. Saturn's rings — particle size distributions for thin layer models. Icarus 64, 531–548.